Angular correlation between photoelectrons and Auger electrons within scattering theory

Fabiana da Pieve, Sergio Di Matteo, Didier Sébilleau, Roberto Gunnella, Giovanni Stefani, Calogero R. Natoli

Angular correlation between photoelectrons and Auger electrons within scattering theory

F. Da Pieve,[1] S. Di Matteo,[2] D. Sébilleau,[3] R. Gunnella,[4] G. Stefani,[1] and C. R. Natoli[2]
[1]*Physics Department, University Roma Tre and CNISM, via della Vasca Navale 84, I-00146 Rome, Italy*
[2]*INFN Laboratori Nazionali di Frascati, via Enrico Fermi 40, I-00044 Frascati, Italy*
[3]*Équipe de Physique des Surfaces et des Interfaces, Laboratoire de Physique des Atomes, Lasers, Molécules et Surfaces, UMR CNRS-Université 6627, Université de Rennes 1, 35042 Rennes Cédex, France*
[4]*Physics Department, University of Camerino, Via Madonna delle Carceri, I-62032 Camerino, Italy*
(Received 3 January 2007; revised manuscript received 22 February 2007; published 3 May 2007)

In this paper we present a single-particle scattering approach for the angular correlation between a photoelectron and the subsequent Auger electron from atomic targets. This method is proposed as an alternative approach with respect to the usual density matrix formalism, since it is more convenient for extension to the solid state case. Such an extension is required by the great progress made in the field of coincidence spectroscopy in condensed matter systems. We derived a tensor expression for the cross section and an equivalent expression in terms of convenient angular functions has been treated for the case of linearly polarized light. Numerical calculations are performed for the $L_3M_{2,3}M_{2,3}$ transition in argon, in the single configuration Dirac-Fock scheme. Results are compared with experimental data for different final angular momentum states of the doubly charged ion and for different kinematical conditions.

DOI: 10.1103/PhysRevA.75.052704 PACS number(s): 32.80.Hd, 31.25.−v

I. INTRODUCTION

During the last two decades differential cross sections describing the ejection of an Auger electron and its related photoelectron have been investigated [1,2], and several experimental results have been published both regarding atomic systems and surfaces [3–7]. Auger-electron–photoelectron coincidence spectroscopy (APECS) exploits the relationship between initial photoionization and subsequent Auger decay, which are related by the respective creation and annihilation of the same core hole. This technique enables the photoemission and Auger spectra to be examined with unprecedented discrimination [8–11].

Coincidence angular distributions contain much information about correlations within the two-electron pair. The difference between the coincidence and single-electron distribution can be considered as an index of the strength of such correlations. The anisotropy in Auger-electron–photoelectron coincidence angular distributions is due both to nonstatistical population in the magnetic sublevels of the intermediate ion caused by photon absorption, which is not probed by single-electron emission, and to the introduction of another quantization axis (the axis of detection of one of the two electrons). Generally, the axial symmetry of the angular distribution with respect to the light quantization axis is broken, and the angular pattern shows different degrees of anisotropy for different detection angles of the first electron. The axial symmetry is retained only if the fixed electron is revealed along the light polarization or along the light propagation direction, depending on the polarization properties of the photon beam. Thus, the study of the symmetry and anisotropy of the angular correlation between the two electrons allows an insight into the interplay between symmetry reduction and interparticle correlation.

From the theoretical point of view the angular correlations between Auger electrons and photoelectrons has been mainly studied using density matrix and statistical-tensor approach [12], or the graphical technique [13]. The statistical-tensor approach, in particular, is very powerful since it allows a many-body treatment of the angular correlation part, with all possible couplings between angular momenta of intermediate or residual final ion and continuum electrons. It is based on rotational invariance of the problem under investigation and therefore it is widely used in atomic physics. It can be applied both to closed and open shell systems and a different coupling scheme can be adopted depending on the relative strength of spin orbit and Coulomb interaction. The Wigner-Eckart theorem leads to a factorization of the cross section in a dynamical and geometrical part, which is very convenient for analyzing the influence of the geometry in different experimental conditions. The general expression for the cross section for Auger-electron–photoelectron coincidence emission can be found in [1]

$$\frac{d^2\sigma}{d\mathbf{k}_A\, d\mathbf{k}_p} = \sum_{k_1 k_2} 4\pi(\hat{k}_1\hat{k}_2)^{-1} A(k_1,k_2,k) \times \{Y_{k_1}(\mathbf{k}_p) \otimes Y_{k_2}(\mathbf{k}_A)\}_{kq} \rho^{\gamma}_{kq}(1,1), \qquad (1)$$

where $\hat{k}=\sqrt{2k+1}$, $\mathbf{k}_p$, $\mathbf{k}_A$ are unit vectors determining the escaping direction of the two outgoing electrons, $\rho^{\gamma}_{kq}(1,1)$ is a dipole photon statistical tensor carrying a total momentum $j_\gamma=1$, and $A(k_1,k_2,k)$ are coefficients which contain all the informations concerning the double photoionization dynamics. When also interference effects such as postcollision interaction (PCI) are considered, then a correlation factor which modifies the angle dependent cross section (1) must be included [15]. For the dynamical parameters many works [16,17] implemented the multiconfiguration Dirac-Fock (MCDF) model with or without QED corrections to calculate radial functions. Coincidence calculations performed within the MCDF approach show good agreement with experimental data, both when reproducing the energy distribution and the angular correlation patterns, even if sometimes a satisfy-

ing agreement in terms of the anisotropy is missing and would require the inclusion of several higher electronic configurations.

In this paper we present an alternative approach for the angular correlation between the two electrons which is based on scattering theory in the single-particle approximation. This approach is entirely based on intuitive concepts of quantum mechanics and has the great advantage that it can also be extended to nonrotationally invariant problems, such as electron scattering in a solid sample, due to the flexibility of scattering theory to treat condensed-matter systems. Therefore, in order to cope with the problem of coincidence angular distributions in condensed matter, one should merge the exact treatment of the angular correlation between the two electrons with the one-particle approach of the multiple scattering theory, which will be described in a forthcoming paper. The boost that coincidence spectroscopy in solid state has received in recent years makes the development of a theoretical method necessary. Our shorter term attempt is to verify if a single-particle approach could give a good description for the angular correlation between the two electrons emitted from an atomic target.

The attention will be focused on the dependence of the angular correlation patterns upon the kinematics of the experiment considered by P. Bolognesi *et al.* [18] and upon angular momentum coupling in the final doubly ionized state. The transition considered is the Ar $L_3M_{23}M_{23}$ transition with photon energy 253.6 eV (only 5 eV above threshold). No distortions of the cross section due to postcollision interaction effects between the photoelectron and the Auger electron (with 200 eV kinetic energy) are included in our simple model. Calculations of radial matrix elements are performed within the single-configuration Dirac-Fock model and results for the coincidence cross section are compared with Auger coincidence angular distributions measured for three different fixed directions of the photoelectron for each final angular momentum state ($^1S_0$, ^3P_J, $^1D_2$).

II. COINCIDENCE CROSS SECTION

The purpose of this section is to present the building blocks for a description of the photoionization and Auger decay process. We are interested in the transition from an initial state given by the ground state of the system plus an incoming photon to a final state with two outgoing electrons and a doubly charged ion. The process of photoionization and Auger decay is energetically degenerate with the so-called direct double photoionization (DPI) process, in which two electrons are simultaneously emitted following the absorption of one photon. In the *t*-matrix approach the general expression for the transition probability is determined by the operator

$$T = D + VG_0T = D + VG_0D + VG_0VG_0T = \sum_{n=0}^{\infty} (VG_0)^n D, \tag{2}$$

which is first order in the dipole operator D and infinite order in the Coulomb decay operator V. In principle one should consider photoinduced Auger electron emission as a resonance embedded in double photoionization, i.e., as a two-electron resonant emission process which interferes with DPI. Then the transition amplitude can be written as

$$T = \langle \psi_{\beta e_1 e_2} | D | \psi_g \rangle + \sum_{\nu} \int \frac{\langle \psi_{\beta e_1 e_2} | V | \Phi_{\nu\tau} \rangle \langle \Phi_{\nu\tau} | D | \psi_g \rangle d\tau}{\epsilon_1 + \epsilon_2 + E_\beta^+ - E_{\nu\tau}}, \tag{3}$$

where ψ_g, $\psi_{\beta e_1 e_2}$ are the ground state and the final state wave functions, the latter given by the doubly ionized ion and the two electrons wave functions. E_β^{++} is the energy of the doubly charged ion and $E_{\nu\tau} \approx E_\nu^+ + \tau - \frac{1}{2} i\Gamma_\nu$ with E_ν^+ being the energy of the one hole ionic state which is coupled to a single-electron excited state $|\tau>$ in the many-electron intermediate state $\Phi_{\nu\tau}$. The first term is DPI. Ignoring the second term is appropriate far from resonances and for such simple systems as He where inner shells do not exist. In the case of excitation and decay of a strong isolated resonance $\nu = r$ (long-lived inner vacancy), one ignores the first term and all terms in the summations over all possible intermediate states except the considered intermediate state. If one then neglects possible final state interactions, and assuming that the difference between the kinetic energies of the two electrons is large compared to the intermediate level width, then the two-step formulation which separates photoionization from Auger decay is obtained as follows:

$$T = \frac{\langle \psi_{\beta e_2}^- | V | \Phi_r \rangle \langle \Phi_{re_1} | D | \psi_g \rangle}{\epsilon_2 + E_\beta^{++} - E_r^+ - \frac{1}{2} i\Gamma_r}. \tag{4}$$

The link between photoionization and Auger decay is made via the intermediate hole state only. Essential prerequisites for the two-step model to be valid are as follows: the intermediate state lifetime must be bigger than the relaxation time of the system (thus, the Auger decay begins from a completely relaxed state so that no influence of the many-body effects due to multiple excitations is observed), a well-defined angular momentum JM and parity, no overlapping with neighbors states, and neglect of direct double photoionization process as well as final channel interactions. For a particular intermediate state the energy denominator is common to all terms and can be factorized giving the standard Lorenz factor $L_\Gamma = (\Gamma_r/2\pi)/[(\epsilon_2 - E_r^+)^2 + \Gamma_r^2/4]$.

In our discussion we adopt a hole picture and the intermediate ion state is denoted only by quantum numbers that characterize the core hole. No further recoupling with higher nonoccupied levels is considered. This is correct in the case of closed shell atoms, but it can be considered valid in more general cases if the spin-orbit interaction of the core hole exceeds the lifetime broadening of the two spin-orbit edges. In the presence of core-outer shell interactions, this approximation is still valid if the energy splitting due to interaction with outer shells does not exceed the lifetime broadening. Moreover, we consider the photoelectron as a pure spectator in the Auger decay neglecting interactions between photoelectron and the core hole state left behind. This is no longer valid if the experiment is performed just above threshold

(photoelectron energy ≈0.02 eV); in this case recoupling between the outgoing electron and the intermediate ion must be considered. Using a hole picture, the ground state is described by one hole in the continuum which will be filled by the photoelectron and the intermediate state by the core hole state. Then the Auger decay starts from the core hole state coupled to one hole in the continuum which will be filled by the Auger electron, and the final state is given by the two holes. In the following we denote e_p, e_A as the photoelectron and the Auger electron, respectively. The spin-orbit coupled core state is given by

$$\psi_c(\mathbf{r}) = R_{nl_c}(r) \sum_{m_c\sigma_c} C^{j_c j_{cz}}_{l_c m_c (1/2)\sigma_c} Y_{l_c m_c}(\hat{\mathbf{r}}) \chi_{\sigma_c}, \tag{5}$$

where χ_{σ_c} are usual spin functions and $C^{j_c j_{cz}}_{l_c m_c \frac{1}{2}\sigma_c}$ are the Clebsch-Gordan coefficients. The one-electron scattering wave-functions solution of the Lippmann-Schwinger equation are given by the time reversed state of the ingoing plane wave

$$\psi_p^- = \Theta \psi^+_{\mathbf{k}_p}(\mathbf{r}_i) = C \sum_{l_p m_p \sigma_p} Y_{l_p m_p}(\mathbf{k}_p) i^{l_p} t_{l_p} R_{\epsilon l_p}(r_i) Y^*_{l_p m_p}(\hat{\mathbf{r}}_i) \Theta \chi_{\sigma_p}, \tag{6}$$

where $t_{l_p} = e^{i\delta_{l_p}} \sin \delta_{l_p}$ describe the strength of the scattering process and δ_{l_p} is the additional phase factor which is acquired by the wave function as a consequence of the scattering potential. C is $\frac{1}{4\pi}\sqrt{\frac{k_p}{\pi}}$ and is given by normalization to one state per Rydberg. The transition operator in dipole approximation can be written in terms of spherical components of $\boldsymbol{\epsilon}$ and $\mathbf{r}$. Then for the dipole matrix element one easily obtains

$$\begin{aligned}\left\langle l_c \tfrac{1}{2} j_c j_{cz} \middle| \boldsymbol{\epsilon} \cdot \mathbf{r} \middle| \psi_p^- \right\rangle &= \sqrt{\frac{k_p}{\pi}} \sum_{\mu} \sum_{l_p m_p \sigma_p m_c} Y^*_{1\mu}(\boldsymbol{\epsilon}) R_{nl_c,\epsilon_p l_p} C^{j_c j_{cz}}_{l_c m_c (1/2)\sigma_p} \\ &\times Y_{l_p m_p}(\mathbf{k}_p) i^{l_p} t_{l_p} \sqrt{\frac{1}{4\pi}} \sqrt{\frac{1}{3}} \frac{\hat{l}_c}{\hat{l}_p} C^{l_p m_p}_{l_c 0 1 0} C^{l_p m_p}_{l_c m_c 1 \mu},\end{aligned} \tag{7}$$

where $R_{nl_c,\epsilon_p l_p}$ is the radial integral. For the second step the initial state for Auger decay can be written as the product of the $\psi_c(\mathbf{r})$ state and the scattering wave function corresponding to the outgoing Auger electron. For the final state, we considered LS coupling to be valid and the two holes wave function can be written as the antisymmetrized product of two particles wave function, where the total orbital L and spin momentum S are coupled to a total J.

The Coulomb interaction can be written as a zero-rank tensor product between spherical harmonics, and integration over angular variables consists in integration over the product of three bipolar spherical harmonics, corresponding to the expansion of the Coulomb interaction and to the intermediate and final state of the process each coupled to a particular orbital momentum. The Auger matrix element, for the case of two equivalent holes, is given by

$$\begin{aligned}&\left\langle [(l_1 l_2) LS] J J_z \middle| \frac{1}{|\mathbf{r}_1 - \mathbf{r}_2|} \middle| \psi_A^-, l_c \tfrac{1}{2} j_c j_{cz} \right\rangle \\ &= \frac{1}{4\pi} \sqrt{\frac{k_A}{\pi}} \hat{l}_1 \hat{l}_2 (-1)^{l_1 + l_c + L} \\ &\times \sum_{l_A k m_A \bar{m}_c \bar{\sigma}_c M S_z} V^k_{n_1 l_1, \epsilon_A l_A, n_c l_c, n_2 l_2} C^{l_A 0}_{l_1 0 k 0} C^{l_c 0}_{l_2 0 k 0} \\ &\times \begin{Bmatrix} l_2 & l_c & k \\ l_A & l_1 & L \end{Bmatrix} C^{J J_z}_{L M S S_z} C^{j_c j_{cz}}_{l_c \bar{m}_c (1/2)\bar{\sigma}_c} \\ &\times C^{L M}_{l_A m_A l_c \bar{m}_c} C^{S S_z}_{(1/2)\sigma_A (1/2)\bar{\sigma}_c} Y_{l_A m_A}(\mathbf{k}_A) i^{l_A} t_{l_A},\end{aligned} \tag{8}$$

where $V^k_{n_1 l_1, \epsilon_A l_A, n_c l_c, n_2 l_2}$ is the Coulomb radial integral (direct and exchange integrals are equal for two equivalent holes; see the Appendix for the more general case). In the intermediate state only the total angular momentum of the core hole is a good quantum number, thus the hole is allowed to migrate to different sublevels m_c, σ_c without changing its total angular momentum and energy. After straightforward though cumbersome applications of angular momentum algebra, we find the following tensor expression for the cross section:

$$\begin{aligned}\frac{d^2\sigma}{d\mathbf{k}_A\, d\mathbf{k}_p} &= 4\pi^2 \alpha \hbar \omega L_\Gamma \sum_{L_0 M_0 l_{pp} l_{AA}} \rho^*_{L_0 M_0} \\ &\times \{ Y_{l_{pp}}(\mathbf{k}_p) \otimes Y_{l_{AA}}(\mathbf{k}_A) \}_{L_0 M_0} A^{L_0}_{l_{pp} l_{AA}},\end{aligned} \tag{9}$$

where $\rho^*_{L_0 M_0} = C^{L_0 M_0}_{1\mu 1\mu'} Y^*_{1\mu}(\boldsymbol{\epsilon}) Y_{1\mu'}(\boldsymbol{\epsilon}^*)$ is the radiation tensor given by combinations of spherical components of the polarization vector, $\{Y_{l_{pp}}(\mathbf{k}_p) \otimes Y_{l_{AA}}(\mathbf{k}_A)\}_{L_0 M_0}$ is the bipolar spherical harmonic which describes the two outgoing electrons, and $A^{L_0}_{l_{pp} l_{AA}}$ (see the Appendix for further details) contains combinations of Clebsch-Gordan, $6j$ and $9j$ coefficients, dipole and Coulomb matrix elements, and the t_l which describe the strength of the scattering for each electron. The angular momentum l_{pp}, l_{AA} are given, respectively, by vector coupling of photoelectron angular momentum l_p and l'_p and Auger electron orbital momentum l_A and l'_A. l_{pp}, l_{AA} are restricted to even values due to parity conservation. Use of the dipole approximation restricts the rank of the radiation tensor only to the values 0,1,2. The same values denote the angular functions which describe the distributions of the two electrons, since the initial target is unpolarized. The spherical tensors approach is more convenient than Cartesian expressions since it allows one to analyze separately which terms contribute to the cross section in different kinematic conditions. In deriving Eq. (10) we could sum up all azimuth quantum numbers except M_0 which reflects the introduction of a preference axis in photon impact. Generalizing this result to the case where the light polarization properties are expressed by Stokes parameters one recovers the result given by the statistical tensor approach for closed shell systems.

Kinematical dependence of the cross section

The purpose of this section is just to give a simple method to obtain an analytical expression for the cross section in order to estimate its angular dependence for different kine-

matic conditions. The cross section describing the two-electron emission must account for all the possible contributions due to the different angular momentum allowed by selection rules. Once a specific model is chosen, the angular correlation between a photoelectron and the Auger electron can be described by a limited set of parameters. Since we are interested in the linearly polarized case, we choose conveniently the reference system with the z axis parallel to the polarization vector. A preliminary analysis can be performed analyzing the order of the spherical harmonics involved in the cross section and writing them as vector and scalar products among the vectors involved in the problem. This allows for a qualitative description just discussing the basic formulas without any detailed calculations.

With linearly polarized radiation, the polarization vector is real, thus $\boldsymbol{\epsilon}^*=\boldsymbol{\epsilon}$ and one can use the addition theorem to recouple the spherical harmonics of the light. Choosing the z axis parallel to the polarization vector, then one has that only the $m_\gamma=0$ spherical components $Y_{10}(\boldsymbol{\epsilon})$ of the polarization vector contribute and only even rank values of the radiation tensor are allowed. The waves describing the photoelectron and the Auger electron have opposite azimuth dependence since they are coupled to $m_\gamma=0$ projections of the light tensor. The cross section is the sum of a simple scalar product between the spherical harmonics of the two electrons (the monopole term) and the zero component of the quadrupole tensor. Following [19] we can define the angular function $F^{L_0}_{l_{pp}l_{AA}}(\mathbf{k}_p,\mathbf{k}_A,\boldsymbol{\epsilon})$ as follows:

$$F^{L_0}_{l_{pp}l_{AA}}(\mathbf{k}_p,\mathbf{k}_A,\boldsymbol{\epsilon}) = \sum_{m_{pp}m_{AA}} C^{L_0 0}_{l_{pp}m_{pp}l_{AA}m_{AA}} Y_{l_{pp}m_{pp}}(\mathbf{k}_p) Y_{l_{AA}m_{AA}}(\mathbf{k}_A) Y_{L_0 0}(\boldsymbol{\epsilon}). \tag{10}$$

Then the cross section can be rewritten as

$$\frac{d^2\sigma}{d\mathbf{k}_A\, d\mathbf{k}_p} = \sum_{L_0 l_{pp} l_{AA}} F^{L_0}_{l_{pp}l_{AA}}(\mathbf{k}_p,\mathbf{k}_A,\boldsymbol{\epsilon}) \tilde{A}^{L_0}_{l_{pp}l_{AA}}, \tag{11}$$

where $\tilde{A}^{L_0}_{l_{pp}l_{AA}} = \frac{3}{2\hat{L}_0} C^{L_0 0}_{1010} 4\pi^2 \alpha \hbar \omega L_\Gamma A^{L_0}_{l_{pp}l_{AA}}$. Thus, the cross section is given by the product of a kinematical part and a dynamical part. We focus our attention on the Auger decay $L_3M_{2,3}M_{2,3}$ in a closed shell system like argon; in dipole approximation and neglecting spin-orbit interaction in the continuum, the photoionization of Ar $2p_{3/2}$ leads to the following possible decays:

$$\begin{aligned} h\nu + \mathrm{Ar} &\rightarrow \mathrm{Ar}^+ 2p^{-1}_{3/2}(^2P_{3/2}) + e^-_p(\boldsymbol{\epsilon}_s,\boldsymbol{\epsilon}_d) \\ &\hookrightarrow \mathrm{Ar}^{2+} 3p^4(^1S_0) + e^-_A(\boldsymbol{\epsilon}_p) \\ &\hookrightarrow \mathrm{Ar}^{2+} 3p^4(^3P_{0,1,2}) + e^-_A(\boldsymbol{\epsilon}_p) \\ &\hookrightarrow \mathrm{Ar}^{2+} 3p^4(^1D_2) + e^-_A(\boldsymbol{\epsilon}_p,\boldsymbol{\epsilon}_f), \end{aligned} \tag{12}$$

where e_p is the photoelectron and e_A the Auger electron. Note that the two holes in the final state can couple their angular momentum in different ways giving different multiplet terms for the final double ion Ar^{2+}; the conservation of total angular momentum and parity leads in this way to different possible partial waves of the Auger electron. The different angular characters of the double ion multiplet term and the different partial waves of the Auger electron affects the angular distribution. The angular momentum allowed by the selection rules are $l_p=0,2$, $l_A=1$ (for final state $^1S_0$ and ^3P_J) and $l_A=1,3$ (for $^1D_2$). The selection rules for l_A can be read easily from Eq. (9), where the $6j$ symbol imposes $|l_c-L| \leqslant l_A \leqslant l_c+L$. For the coupled quantum numbers $l_{pp}=0,2,4$, $l_{AA}=0,2$, $L_0=0,2$. Regarding the k index in Eq. (8), which expresses the expansion index for the Coulomb interaction, in the case of the transition considered, it can assume the values $k=0,2$, while only $k=2$ is possible when $l_A=3$ ($^1D_2$). Thus, the differences in the angular distributions related to the different final states are mainly given by the angular momentum of the final state and the possible angular momenta allowed for the Auger electron, since the k terms are nearly the same for all states, except the $k=2$ term (for $l_A=3$) in the decay path to $^1D_2$. Of course, also small differences in the matrix elements due to slightly different kinetic energies of Auger electrons related to the final possible ion states can appear but such differences can be neglected. The allowed angular function $F^{L_0}_{l_{pp}l_{AA}}$ are $F^0_{00}, F^0_{22}, F^2_{02}, F^2_{20}, F^2_{22}, F^2_{42}$, and some of them are listed below as follows:

$$F^0_{22} \propto 3(\mathbf{k}_p\cdot\mathbf{k}_A)^2 - 1, \tag{13}$$

$$F^2_{22} \propto 2 - 3(\mathbf{k}_A\cdot\boldsymbol{\epsilon})^2 - 3(\mathbf{k}_p\cdot\boldsymbol{\epsilon})^2 - 3(\mathbf{k}_p\cdot\mathbf{k}_A)^2 + 9(\mathbf{k}_A\cdot\mathbf{k}_p) \times (\mathbf{k}_A\cdot\boldsymbol{\epsilon})(\mathbf{k}_p\cdot\boldsymbol{\epsilon}), \tag{14}$$

$$F^2_{42} \propto 1 - 5(\mathbf{k}_A\cdot\boldsymbol{\epsilon})^2 + 2(\mathbf{k}_p\cdot\boldsymbol{\epsilon})^2 - 5(\mathbf{k}_p\cdot\mathbf{k}_A)^2 - 20(\mathbf{k}_A\cdot\mathbf{k}_p) \times (\mathbf{k}_A\cdot\boldsymbol{\epsilon})(\mathbf{k}_p\cdot\boldsymbol{\epsilon}) + 35(\mathbf{k}_A\cdot\mathbf{k}_p)^2(\mathbf{k}_p\cdot\boldsymbol{\epsilon})^2. \tag{15}$$

The angular functions F^2_{02}, F^2_{20} are equal to the first one F^0_{22} but with $(\mathbf{k}_A\cdot\boldsymbol{\epsilon})^2$ and $(\mathbf{k}_p\cdot\boldsymbol{\epsilon})^2$ instead of $(\mathbf{k}_p\cdot\mathbf{k}_A)^2$. F^0_{00} is a constant.

If the photoelectron is detected along the light polarization vector, then the cross section is proportional to $A+B(\cos\theta_A)^2$ like in a conventional one-electron experiment. The same angular dependence is obtained when the Auger electron is detected along the polarization vector. If one detects the photoelectron perpendicular to the polarization vector, then some angular functions $F^{L_0}_{l_{pp}l_{AA}}$ do not contribute (for example, the F^2_{20} with its corresponding dynamical part A^2_{20} and some terms in F^2_{22} and in F^2_{42}). In different geometries the dynamical part $\tilde{A}^{L_0}_{l_{pp}l_{AA}}$ is weighted in different ways. For example, subtracting the cross sections measured with $\mathbf{k}_p$ parallel and perpendicular to $\boldsymbol{\epsilon}$, then we can single out the contribution of dynamical and angular parts related to different waves describing the continuum electrons. Therefore, one can inspect the behavior of the angular functions $F^{L_0}_{l_{pp}l_{AA}}$ allowed for the transition of interest in order to choose a geometry which suppresses contributions from certain angular components for the continuum electrons. It is clear that varying the detection angle of the first electron, the degree of anisotropy of the angular distribution of the second electron is different. Thus, the expression (11) for the cross section is

convenient in order to analyze what is the expected angular dependence for a particular geometry of the experiment and for a particular transition.

III. NUMERICAL CALCULATIONS

Both bound state and excited radial wave functions have been calculated using the PHAGEN code which uses a single configuration Dirac-Fock implementation of Desclaux's program [20,21]. In the single configuration Dirac-Fock, a state function is given by a Slater determinant of the Dirac orbitals. Our code includes the Breit interaction—Gaunt term +retardation term–only as a first-order perturbative correction (after the self-consistent iterations converged with the Coulomb interaction terms only). Then the code generates the radial matrix elements and the t_l elements which contain the phase shifts and describe the strength of the interaction.

The initial wave functions are obtained by integration of the Dirac equation using a self-consistent procedure. Exchange and correlation potential can be included using various approximations for the final state. In our case the Hedin-Lundqvist [22] exchange correlation potential has been used. For the calculations of the matrix elements, different widths of the Auger peaks corresponding to the different final angular momentum states due to photoionization above threshold have been taken into account. The cross section is then calculated using the SPEC [23] package, which calculates all the angular momentum coefficients and performs the necessary external and coherent summations over quantum numbers. This package is a multiple scattering package for treating emission from a solid sample, but the multiple scattering part can be externally switched off and then the atomic distribution is calculated.

IV. RESULTS AND DISCUSSION

For each multiplet term of the final ion state three coincidence angular distributions have been analyzed, corresponding to photoelectron detection at 0°, 30°, 60° from the polarization direction in the plane of detection of the two electrons perpendicular to the photon beam. Normalization between theory and experimental data has been performed by comparing the integrated cross section and scaling the theoretical results using the ratio between the two integrals.

The comparison between experimental data and theoretical curves for $^1S_0$ final state is presented in Fig. 1. The agreement is good for the experimental condition in which the photoelectron is revealed along the light polarization vector. In this case no additional quantization axis are introduced and the angular distribution of coincident Auger electrons retains its axial symmetry with respect to the light polarization direction. In this case also the anisotropy is reproduced well by the theoretical calculations. When the direction of detection of the first electron is moved to 30° from the polarization vector, the calculations seem to reproduce still rather well the position of the lobes observed in the experiments, but the theoretical predictions appear to be more anisotropic than the measurements. We remember that in our model no PCI effects are taken into account. However, it is not possible to say *a priori* which consequences these effects could have on the cross section in terms of an enhanced or reduced anisotropy. A more complete treatment of the inter-

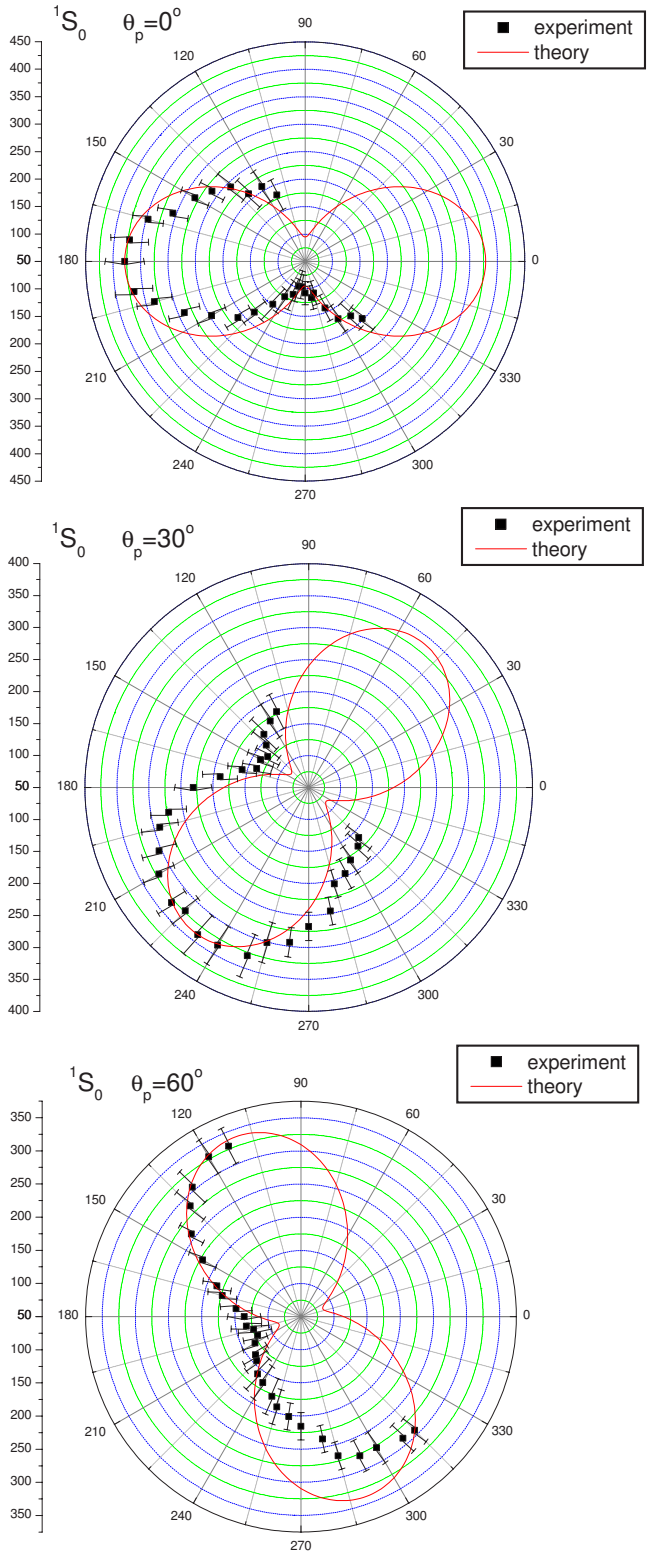

FIG. 1. (Color online) Comparison between experimental data and theoretical results for Ar $L_3M_{2,3}M_{2,3}$ ($^1S_0$) Auger coincidence angular distributions for different detection angles of the photoelectron (θ_p=0°, θ_p=30°, θ_p=60°). Both electrons are detected in the plane perpendicular to the photon beam.

mediate state should improve the agreement between the theoretical results and the experimental data, but it is not possible to affirm that PCI effects would surely reduce the anisotropy. The discrepancy concerning the anisotropy appears also in the case when the photoelectron is detected at 60° from the polarization. In this latter condition also a disagreement in reproducing the lobe at ≈300° can be noted. In contrast to the two previous cases ($\theta_p=0°$ and $\theta_p=30°$), the experimental results are dissymmetrical. Agreement with the upper experimental lobe is good, while that with the lower one is not. This discrepancy has quite a strange character, since the calculations seem to reproduce the position of the lobe quite well but overestimate its intensity. A distorted angular distribution can be induced in cases in which PCI effects are important. In the experiment the photon energy was just 5 eV above the Ar L_3 threshold, thus the photoelectron has a much lower energy with respect to the Auger electron, and some interference effects could arise, i.e., the photoelectron with its lower energy acts as a postcollision effect inducer for the process of Auger electron emission. This could lead to distortions of the coincidence cross section. However, to test if such effects are present or not, one should improve the experiment with better statistics and measurements over a larger angular range.

Analytical expressions for the cross sections in the different experimental geometries and for the different decay paths have been derived implementing the "modulus square" formulation of the intensity [given by the product between Eqs. (7) and (9)] using MATHEMATICA 5.0 [14]. They are obtained very quickly with respect to calculations performed using the tensor representation of the cross section, because of the presence of several Wigner nj symbols in the dynamical factor whose calculation is time consuming. Checks to test the equivalence between the modulus square and the tensor formulation have been done (and they prove the correctness of the angular momentum recouplings). Considering the reference system with the z axis along the beam polarization and the y axis along the beam propagation direction, the analytical expressions for the angular distributions presented in Fig. 1 are given by (both $\phi_p=\phi_A=0°$)

$$\left.\frac{d\sigma}{d\theta_A}\right|_{\theta_p=0°} \propto 3.46\cos^2\theta_A + 0.87\sin^2\theta_A,$$

$$\left.\frac{d\sigma}{d\theta_A}\right|_{\theta_p=30°} \propto 1.86 - 0.23\cos 2\theta_A + 1.09\sin 2\theta_A,$$

$$\left.\frac{d\sigma}{d\theta_A}\right|_{\theta_p=60°} \propto 1.25 - 0.60\cos 2\theta_A - 0.46\sin 2\theta_A. \tag{16}$$

The weights of the sine and cosine functions are given by angular momentum coefficients and matrix elements which govern the transition. In principle, for more complex distributions, one could use the analysis provided by the $F^{L_0}_{l_{pp'}l_{AA}}(\mathbf{k}_p,\mathbf{k}_A,\boldsymbol{\epsilon})$ functions to suppress some terms in the cross section. In our case, we did not consider the spin-orbit interaction in the continuum, and thus a comparison between extracted and calculated photoionization matrix elements related to $l_p=0$, $j_p=1/2$ and $l_p=2$, $j_p=3/2$; 5/2 is not feasible and beyond the scope of this work. Moreover, since in this decay path only one angular momentum is allowed for the Auger electron ($l_A=1$), and since the $l_p=2$ is dominant with respect to the lower channel $l_p=0$ (an order of magnitude of difference), both dipole and Coulomb matrix elements can be factorized (the latter for a determined k index), leading to an expression for the cross section which is the sum of the k_0 and k_2 terms. The ratio between the two integrals $|D_{k=0}|/|D_{k=2}|$ is 1.4. Thus, it is true that $k=0$ is the leading term, but also the term related to $k=2$ cannot be neglected. This complete factorization of the dipole matrix element and the partial factorization of the Coulomb matrix element means that the angular part of the cross section describes well the correlation between the two electrons, as seen by the agreement with the experimental data.

In Fig. 2 the comparison between theoretical calculations and experimental data for the ^3P_J final state is reported. Since the different spin-orbit component J of the final ion state are not resolved experimentally, we summed over the theoretical contributions from the different values of J with their statistical weights. It can be observed that for all the angular distributions (photoelectrons detected at 0°, 30°, 60° from the light polarization vector) the positions of the peaks are well reproduced while the anisotropy of the calculations is more pronounced than that of the experimental data. The discrepancy is larger at a large angle between the light polarization and the direction of detection of the photoelectron. It can be noted that, especially in the case in which the photoelectron is detected at $\theta_p=0°$ and $\theta_p=60°$, the experimental data behave in a different way from what is expected, since in the position of the theoretical minimum the measurements seem to have a slight increase in intensity. These structures are far from being possible additional lobes, but the effect is clear and probably more evident in the condition $\theta_p=0°$ where at 180° a secondary local maximum appears in the experimental data. The theory only reproduces the two main structures in the cross section and completely misses such extra structures with lower intensity. The reason for this discrepancy between theory and experiments could again rely on the neglected PCI effects in the model calculations. PCI effects are known to eventually predict a collapse of the angular pattern for small relative angle between the two electrons [15], but here no experimental data for the Auger electron are present near $\theta_p=0°$. The slight increase in the intensity appears exactly when the two electrons are measured in opposite directions. Moreover, these structures are not present in the case of $^1S_0$ and $^1D_2$ final state. This could suggest that the triplet character of the two electrons wave functions in the case of ^3P_J could lead to differences with respect to a singlet emission case due to exchange effects, apart from considering the whole rotation of the angular distribution which is different for each decay path. The unclear origin of this behavior should be further investigated.

The analytical expressions for the angular distributions for the ^3P_J final state are given by Eq. (10) as follows:

$$\left.\frac{d\sigma}{d\theta_A}\right|_{\theta_p=0^\circ} \propto 2.48 + 0.91\cos 2\theta_A,$$

$$\left.\frac{d\sigma}{d\theta_A}\right|_{\theta_p=30^\circ} \propto 1.74 - 0.63\sin 2\theta_A,$$

$$\left.\frac{d\sigma}{d\theta_A}\right|_{\theta_p=60^\circ} \propto 1.04 + 0.25\cos 2\theta_A + 0.26\sin 2\theta_A. \tag{17}$$

Also in the case of ^3P_J there is only one value of the angular momentum allowed for the Auger electron ($l_A=1$). This means again that both the dipole and Auger matrix elements can be factorized (the former due to the fact that the $l_p=2$ channel is dominant with respect to the $l_p=0$ term). Thus, the angular part is the only part which really describes the correlation between the two electrons, except for the weights given by the two terms corresponding to $k=0$ and $k=2$ of the related Auger matrix elements.

In Fig. 3 we present the comparison between the experimental data and the theoretical calculations for the $^1D_2$ final state. As can be seen, also in this case the calculations reproduce well the shift of the coincidence angular distributions with respect to the light polarization vector. The positions of the lobes agree in all three kinematic conditions, while the anisotropy is not well reproduced in every kinematic condition. In the other cases the theoretical angular distributions are more anisotropic than the experimental patterns, especially when $\theta_p=30^\circ$ from the polarization. No other structures seem to be present in the experimental data, contrary to the case of the ^3P final state. However, in the case $\theta_p=0^\circ$ the experimental cross section seems not to have the simple form predicted by theory. Such a disagreement goes beyond the anisotropic problem and should be investigated at different photon energy to assess its origin.

The analytical expressions for the angular distributions for the $^1P_2$ state are given by

$$\left.\frac{d\sigma}{d\theta_A}\right|_{\theta_p=0^\circ} \propto 4.06 + 4.32\cos 2\theta_A + 0.81\cos 4\theta_A + 0.12\cos 6\theta_A,$$

$$\left.\frac{d\sigma}{d\theta_A}\right|_{\theta_p=30^\circ} \propto 2.83 + 1.82\cos 2\theta_A + 0.07\cos 4\theta_A + 0.05\cos 6\theta_A + 2.37\cos\theta_A\sin\theta_A + 0.45\sin 4\theta_A + 0.04\sin 6\theta_A,$$

$$\left.\frac{d\sigma}{d\theta_A}\right|_{\theta_p=60^\circ} \propto 1.68 + 0.60\cos 2\theta_A - 0.15\cos 4\theta_A + 0.11\cos 6\theta_A - 0.98\cos\theta_A\sin\theta_A - 0.19\sin 4\theta_A - 0.18\sin 6\theta_A. \tag{18}$$

These expressions are more complicated than those related to the $^1S_0$, ^3P_J final states, since for the $^1D_2$ final state also the $l_A=3$ is possible for the Auger electron. When $l_A=3$ only $k=2$ is possible, and the corresponding radial integral has nearly the same absolute value of the term $l_A=1$, $k=2$, but with opposite sign. Thus, in this case no factorization

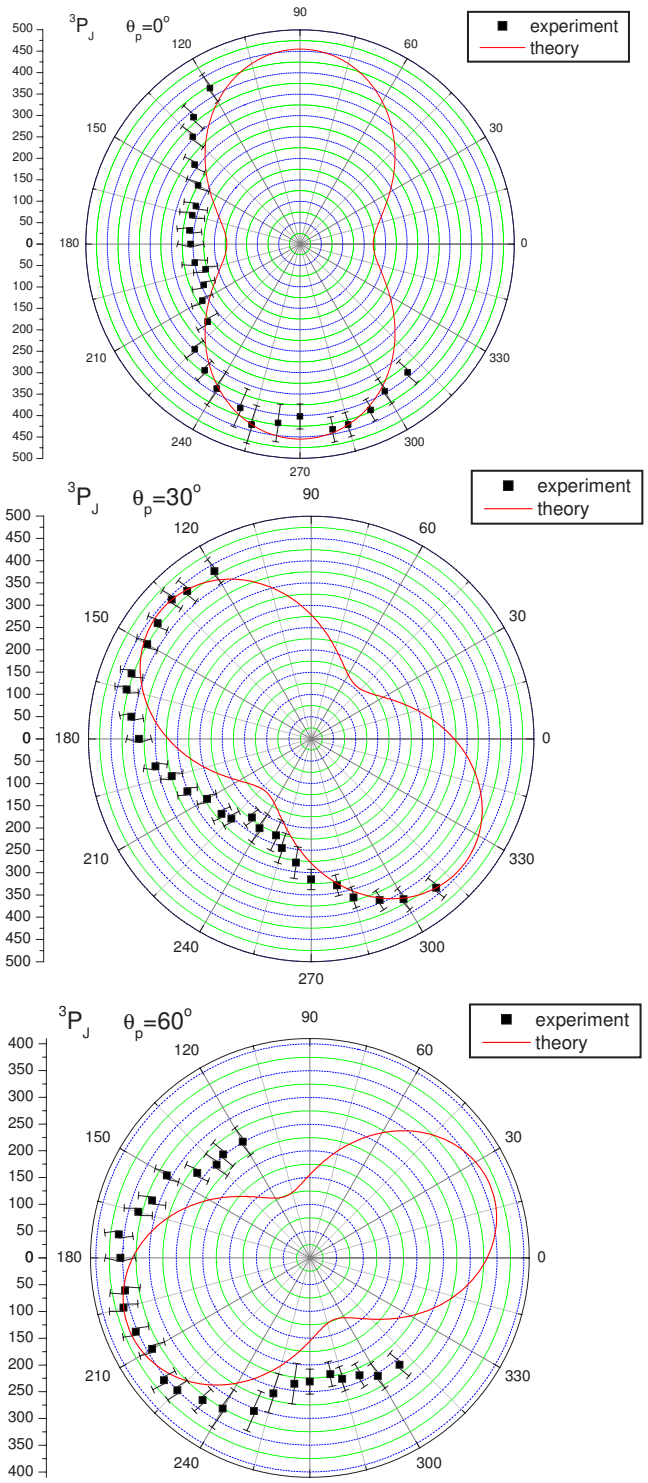

FIG. 2. (Color online) Comparison between experimental data and theoretical results for Ar $L_3M_{2,3}M_{2,3}$ (^3P_J) Auger coincidence angular distributions for different detection angles of the photoelectron ($\theta_p=0^\circ$, $\theta_p=30^\circ$, $\theta_p=60^\circ$). Both electrons are detected in the plane perpendicular to the photon beam.

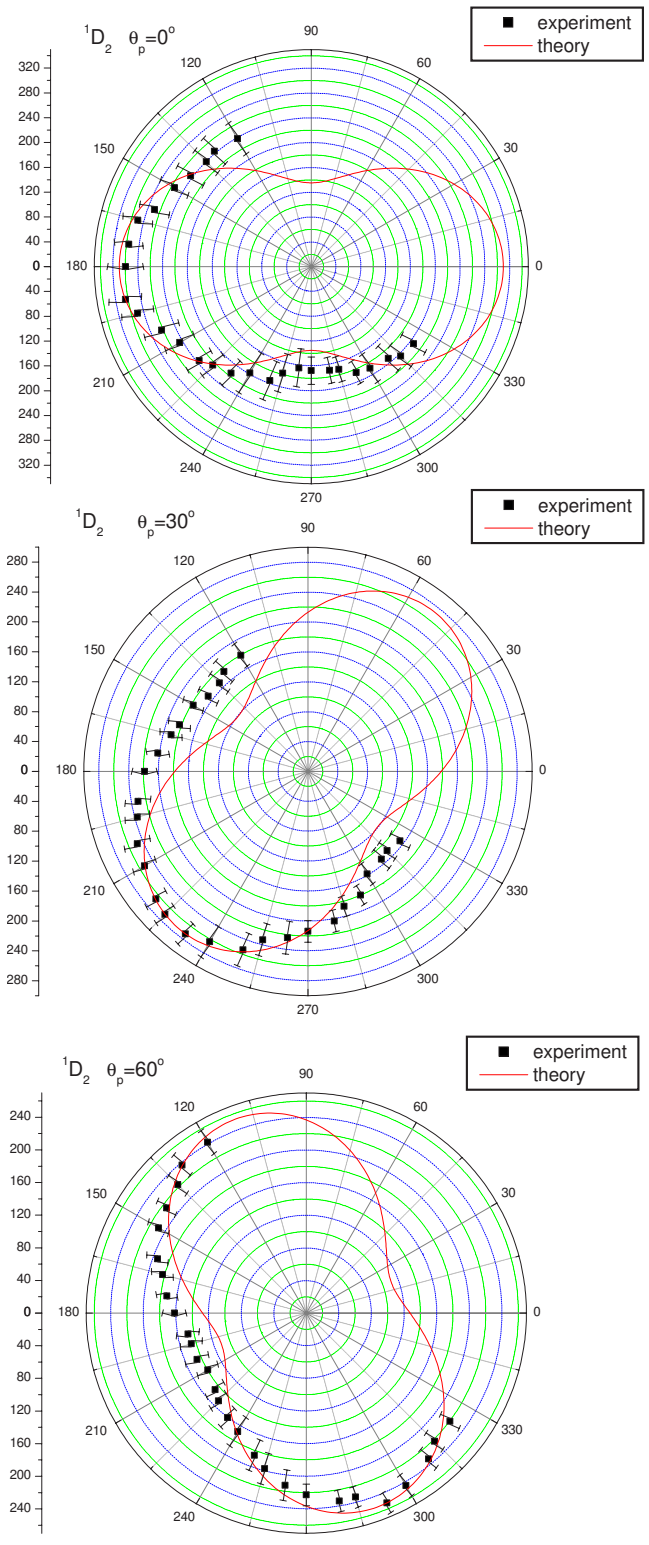

FIG. 3. (Color online) Comparison between experimental data and theoretical results for Ar $L_3M_{2,3}M_{2,3}$ ($^1D_2$) Auger coincidence angular distributions for different detection angles of the photoelectron (θ_p=0°, θ_p=30°, θ_p=60°). Both electrons are detected in the plane perpendicular to the photon beam.

for the Coulomb matrix elements can be done and the cross section has a more complicated form due to the interference between these two channels.

V. CONCLUSIONS

In this paper we have presented a scattering approach for the angular correlation between the photoelectron and the subsequent Auger electron based on a single-particle scheme. This method is proposed as an alternative approach with respect to the usual density matrix formalism, since it is more convenient for an extension to the solid state case. It could also allow one to merge a correct description of the two-electrons correlation with the fundamental spectra formalism given by Thole and van der Laan [24–26] for several spectroscopies, which has proved to be very useful in the interpretation of light properties dependence of the corresponding cross sections. We derived a tensor expression for the cross section and an equivalent expression in terms of convenient angular functions has been treated for the case of linearly polarized light. The agreement between theoretical calculations and experimental data for Ar $L_{23}M_{23}M_{23}$ Auger transition depends on the specific decay path and the photoelectron's direction. Regarding the geometry of the experiment, for all possible ion final states the agreement in anisotropy decreases when the photoelectron is moved from the light polarization direction. For the position of the peaks some discrepancy appears, especially in the $^1S_0$, θ_p=60° case. However, the agreement is of the same order as in the case of other calculations performed within the statistical tensor approach used in angular correlations problems, where all possible angular momentum recoupling are considered and matrix elements are usually calculated using the MCDF model. Disagreement in terms of anisotropy of the angular distributions can be noted in both approaches. This can be due to a wrong description of the intermediate state. Regarding distortions which appear in the cross section which is not clearly explainable, one could argue that PCI effects could arise due to the lower kinetic energy of the photoelectron, even if this is not the only possibility for disagreement. However, PCI effects generally induce some collapses of the correlation patterns at small relative angles (where no experimental data are available) due to repulsive interaction between the two electrons. Experimental data should be collected over a larger angular range in order to test the presence of such effects. Both additional experimental and theoretical efforts are necessary in order to clarify the situation.

In the case of emission from molecules and clusters, the outgoing electron wave functions are expanded in curved waves, and this brings further summations which should be added to those due to selection rules of the process. Indeed, due to the breaking of the spherical symmetry in the solid state, the emitted electron will not be described by eigenfunctions of the orbital momentum anymore, but a different description must be used. The multiple scattering events felt by the two electrons could even obscure completely the initial angular correlation between the two electrons at the atomic site. The possibility to extend the theoretical treatment of the two-electron correlation to solid state is very attractive since it could allow one to interpret the coincidence experiments whose results have been published in recent years. Extension to the case of Auger-electron–

photoelectron pairs emitted from a cluster becomes necessary and it will be treated elsewhere.

ACKNOWLEDGMENTS

We wish to acknowledge the group of P. Bolognesi and L. Avaldi (IMIP-CNR-Rome) for having provided us the experimental data to which our calculations have been compared. This work has been supported by the MIUR-PRIN 2005 "Highly correlated low dimensional systems studied by coincidence electron spectroscopies: A new generation of experimental and theoretical methods funds".

APPENDIX: FORM OF THE DYNAMICAL PART OF THE CROSS SECTION

In this appendix we hint at some steps of the calculations without going into the full details. The coincidence cross section is given by the modulus square of the product between Eqs. (7) and (8), with equal intermediate quantum numbers in the two steps of the process, and with an external sum over the two spin projections of the continuum electrons and over the magnetic quantum number of the residual ion as follows:

$$\frac{d^2\sigma}{d\mathbf{k}_A\, d\mathbf{k}_p} = 4\pi^2\alpha\hbar\omega\Gamma \sum_{\sigma_A\sigma_p J_z} \left| \frac{e^2}{\sqrt{2}}\sqrt{\frac{4\pi}{3}}\left(\frac{1}{4\pi}\right)^2 \sqrt{\frac{k_A}{\pi}}\sqrt{\frac{k_p}{\pi}}\hat{l}_1\hat{l}_2\hat{l}_c(-1)^{l_c+l_1+L} \sum_{l_p l_A \mu k} \frac{1}{\hat{l}_p} Y^*_{1\mu}(\boldsymbol{\epsilon}) R(n_c l_c, E l_p) \right.$$
$$\times [D^k_{n_1 l_1 n_2 l_2, \epsilon l_A n_c l_c} d_{k l_A} + (-1)^{-L-S} E^k_{n_2 l_2 n_1 l_1, \epsilon l_A n_c l_c} e_{k l_A}] \sum_{m_A m_c m_p M S_z \bar{m}_c \bar{\sigma}_c j_{cz}} C^{l_p 0}_{l_c 0 1 0}$$
$$\left. \times\, C^{l_p m_p}_{l_c m_c 1\mu} C^{JJ_z}_{LMSS_z} C^{j_c j_{cz}}_{l_c m_c (1/2)\sigma_p} C^{j_c j_{cz}}_{l_c \bar{m}_c (1/2)\bar{\sigma}_c} C^{LM}_{l_A m_A l_c \bar{m}_c} C^{SS_z}_{1/2\, \bar{2}\sigma_A (1/2)\bar{\sigma}_c} Y_{l_A m_A}(\mathbf{k}_A) Y_{l_p m_p}(\mathbf{k}_p) i^{l_p + l_A} t_{l_A} t_{l_p} \right|^2, \tag{A1}$$

where we have used the notation $D_k(n_1 l_1 n_2 l_2, \epsilon l_A n_c l_c)$ for direct Coulomb radial matrix elements and $E_k(n_2 l_2 n_1 l_1, \epsilon l_A n_c l_c)$ for the exchange Coulomb radial matrix element. The coefficient d_{kl_A} and e_{kl_A} comes from the integration over the spherical harmonics and are given by the corresponding Gaunt coefficients.

The photoelectron is considered as a spectator in the second step decay. Starting from Eq. (A1) one can simplify first coupling the Clebsch-Gordan coefficients eliminating the projections j_{cz}, j'_{cz}, σ_A, J_z (the primed numbers are those due to interference), as, for example,

$$\sum_{j_{cz}} C^{j_c j_{cz}}_{l_c m_c (1/2)\sigma_p} C^{j_c j_{cz}}_{l_c \bar{m}_c (1/2)\bar{\sigma}_c} = \sum_{c\gamma} (-1)^{c + j_c + \bar{m}_c - \sigma_p} \hat{j}_c^2 C^{c\gamma}_{l_c m_c l_c - \bar{m}_c} C^{c\gamma}_{1/2 - \sigma_p (1/2)\bar{\sigma}_c} \begin{Bmatrix} l_c & l_c & c \\ \frac{1}{2} & \frac{1}{2} & j_c \end{Bmatrix}. \tag{A2}$$

Performing such couplings then the way to proceed is made clearer and summations over the spin projections of the photoelectron and residual ion can be performed. Then one comes to an expression which contains two bipolar spherical harmonics (the second one appears as a consequence of the interference). Due to rotational invariance, they can be coupled further to a third spherical harmonic denoted by quantum numbers which then result to be the one related to the photon beam properties (since the initial atom is unpolarized and is a closed shell system, the moment induced by beam impact is directly transferred to the two-electron pair) as follows:

$$\{Y_{l_p}(\mathbf{k}_p) \otimes Y_{l_A}(\mathbf{k}_A)\}_{L_1 M_1} (-1)^{M_2} (-1)^{l'_A + l'_p - L_2} \{Y_{l'_p}(\mathbf{k}_p) \otimes Y_{l'_A}(\mathbf{k}_A)\}_{L_2 - M_2}$$
$$= (-1)^{l'_A + l'_p - L_2 + M_2} \sum_{L_3 M_3} C^{L_3 M_3}_{L_1 M_1 L_2 - M_2} \sum_{l_{pp} l_{AA}} \frac{\hat{l}_p \hat{l}'_p \hat{l}_A \hat{l}'_A \hat{L}_1 \hat{L}_2}{4\pi} C^{l_{pp}0}_{l_p 0 l'_p 0} C^{l_{AA}0}_{l_A 0 l'_A 0} \begin{Bmatrix} l_p & l'_p & l_{pp} \\ l_A & l'_A & l_{AA} \\ L_1 & L_2 & L_3 \end{Bmatrix} \{Y_{l_{pp}}(\mathbf{k}_p) \otimes Y_{l_{AA}}(\mathbf{k}_A)\}_{L_3 M_3}. \tag{A3}$$

The $A^{L_0}_{l_{pp} l_{AA}}$ factor in the tensorial cross section (9) is given by

$$A^{L_0}_{l_{pp} l_{AA}} = \hat{j}_c^2 \hat{j}'^2_c \hat{J}^2 \hat{S}^2 \hat{l}_c^2 \hat{l}_1^2 \hat{l}_2^2 e^4 |k_A||k_p| \frac{2}{3\pi} \frac{1}{(16\pi^2)^2} \sum_{\mu\mu' l_A l'_A l_p l'_p k k'} \frac{1}{l_p l'_p} Y^*_{1\mu}(\hat{\epsilon}) Y_{1\mu'}(\hat{\epsilon}^*) R_{n_c l_c, E l_p} R^*_{n_c l_c, E l'_p} C^{l_p 0}_{l_c 0 1 0} C^{l'_p 0}_{l_c 0 1 0}$$
$$\times [D^k_{n_1 l_1 n_2 l_2, \epsilon l_A n_c l_c} d_{k l_A} + (-1)^{-L-S} E^k_{n_2 l_2 n_1 l_1, \epsilon l_A n_c l_c} e_{k l_A}][D^{k'^*}_{n_1 l_1 n_2 l_2, \epsilon l'_A n_c l_c} d_{k' l'_A} + (-1)^{-L-S} E^{k'^*}_{n_2 l_2 n_1 l_1, \epsilon l'_A n_c l_c} e_{k' l'_A}]$$
$$\times \sum_{cgfpr L_e L_1 L_2} (-1)^{-p+g+r+L_e-L_0+l'_A+l'_p} \hat{g}^2 \hat{f}^2 \hat{p}^2 \hat{c}^2 \hat{r}^2 \hat{L}_e^2 \hat{L}_1^2 \hat{L}_2^2 \begin{Bmatrix} \frac{1}{2} & \frac{1}{2} & g \\ c & f & \frac{1}{2} \end{Bmatrix} \begin{Bmatrix} l_c & l_c & c \\ \frac{1}{2} & \frac{1}{2} & j_c \end{Bmatrix} \begin{Bmatrix} l_c & l_c & g \\ \frac{1}{2} & \frac{1}{2} & j_c \end{Bmatrix} \begin{Bmatrix} S & S & f \\ \frac{1}{2} & \frac{1}{2} & \frac{1}{2} \end{Bmatrix}$$

$$\times \begin{Bmatrix} L & L & f \\ S & S & J \end{Bmatrix} \begin{Bmatrix} L & 1 & p \\ l_c & l_c & c \end{Bmatrix} \begin{Bmatrix} L & 1 & r \\ l_c & l_c & g \end{Bmatrix} \begin{Bmatrix} 1 & 1 & L_0 \\ L & L & f \\ r & p & L_e \end{Bmatrix} \sum_{l_{pp} l_{AA} M_0} \frac{\hat{l}_p \hat{l}'_p \hat{l}_A \hat{l}'_A}{4\pi} C^{l_{pp}0}_{l_p 0 l'_p 0} C^{l_{AA}0}_{l_A 0 l'_A 0} \begin{Bmatrix} l_p & l'_p & l_{pp} \\ l_A & l'_A & l_{AA} \\ L_1 & L_2 & L_0 \end{Bmatrix}$$

$$\times \{Y_{l_{pp}}(\mathbf{k}_p) \otimes Y_{l_{AA}}(\mathbf{k}_A)\}_{L_0 M_0} i^{l_p + l_A - l'_p - l'_A} t_{l_A} t_{l_p} t^*_{l'_p} t^*_{l'_A}. \tag{A4}$$

All the intermediate quantum numbers (c,g,f,p,r) which appear in Eq. (A4) are due to summations over magnetic quantum numbers of the electrons involved in the whole process. The only magnetic quantum number which still appears in the cross section is the one related to the introduction of a preference axis (the light polarization or the beam propagation direction). The $A^{L_0}_{l_{pp} l_{AA}}$ contains the dynamical properties (i.e., radial matrix elements and their phase shifts) which weight in a different way the allowed angular momentum components for the continuum wave functions.

[1] N. M. Kabachnik, J. Phys. B **25**, L389 (1992).
[2] B. Kämmerling and V. Schmidt, J. Phys. B **26**, 1141 (1993).
[3] B. Kämmerling and V. Schmidt, Phys. Rev. Lett. **67**, 1848 (1991); **69**, 1145 (1992).
[4] A. De Fanis, J. Phys. B **32**, 5739 (1999).
[5] A. De Fanis, H.-J. Beyer, K. J. Ross, and J. B. West, J. Phys. B **34**, L99 (2001).
[6] R. Gotter, A. Ruocco, M. T. Butterfield, S. Iacobucci, G. Stefani, and R. A. Bartynski, Phys. Rev. B **67**, 033303 (2003).
[7] R. Gotter, F. Da Pieve, A. Ruocco, F. Offi, G. Stefani, and R. A. Bartynski, Phys. Rev. B **72**, 235409 (2005).
[8] W. S. M. Werner, Surf. Interface Anal. **23** 737 (1995).
[9] R. Gotter, W.-K. Siu, R. A. Bartynski, S. L. Hulbert, Xilin Wu, M. Zitnik, and H. Nozoye, Phys. Rev. B **61** 4373 (2000).
[10] E. Jensen, R. A. Bartynski, S. L. Hulbert, E. D. Johnson, and R. Garrett, Phys. Rev. Lett. **62**, 71 (1989).
[11] S. M. Thurgate and Z. T. Jiang, Surf. Sci. **466** L807 (2000).
[12] V. V. Balashov, A. N. Grum-Grzhimailo, and N. M. Kabachnik, *Polarization and Correlation Phenomena in Atomic Collisions* (Kluwer Academic/Plenum Publishers, New York, 2000).
[13] A. Kuplianskiene and V. Tutlys, Phys. Scr. **67**, 290 (2003).
[14] http://www.wolfram. com/products/mathematica.html
[15] N. Scherer, H. Lörch, T. Kerkau, and V. Schmidt, J. Phys. B **37**, L121 (2004).
[16] K. Ueda, Y. Shimizu, H. Chiba, M. Kitajima, H. Tanaka, S. Fritzsche, and N. M. Kabachnik, J. Phys. B **34**, 107 (2001).
[17] F. Da Pieve, L. Avaldi, R. Camilloni, M. Coreno, G. Turri, A. Ruocco, S. Fritzsche, N. M. Kabachnik, and G. Stefani, J. Phys. B **38**, 3619 (2005).
[18] P. Bolognesi, A. De Fanis, M. Coreno, and L. Avaldi, Phys. Rev. A **70**, 022701 (2004).
[19] B. T. Thole and G. van der Laan, Phys. Rev. B **49**, 9613 (1994).
[20] J. P. Desclaux, Comput. Phys. Commun. **9**, 31 (1975).
[21] A. L. Ankudinov, S. I. Zabinsky, and J. J. Rehr, Comput. Phys. Commun. **98**, 359 (1996).
[22] L. Hedin and S. Lundqvist, in *Solid State Physics*, edited by F. Seitz, D. Turnbull, and H. Ehrenreich (Academic, New York, 1969), p. 1.
[23] SPEC code by D. Sébilleau (multiple scattering code for photoelectron, Auger electron diffraction, and APECS). Available upon request (didier.sebilleau@univ-rennes1.fr)
[24] B. T. Thole and G. van der Laan, Phys. Rev. B **49**, 9613 (1994).
[25] B. T. Thole and G. van der Laan, Phys. Rev. B **44**, 12424 (1991).
[26] B. T. Thole and G. van der Laan, Phys. Rev. Lett. **70**, 2499 (1993).